Applicability of Two-step Homogenization in High-crimp Woven Composites

HIGOR GALDINO DA SILVA and BORYS DRACH

ABSTRACT

In the present work, we analyze the applicability of two-step homogenization applied to 3D woven composites with high crimp reinforcement. The available micromechanical homogenization approaches (Hashin, Chamis, Hashin-Shtrikman bounds etc.) were developed and validated for unidirectional composites. These formulas have also been used by the community to homogenize tows in 2D and 3D woven composites including reinforcement architectures with high crimp ratios. However, a rigorous study of their applicability to high-crimp geometries is yet to be performed.

We utilize Finite Element Analysis (FEA) to calculate the overall engineering constants (Young's moduli and shear moduli) of tows having various crimp (CR) and wavelength-to-fiber diameter (λ/d) ratios. For this analysis, periodic sinusoidal unit cells following shapes of individual fibers are used. Fiber volume fraction is set to 70% and is the same in all cases. Transversely isotropic carbon fiber and isotropic epoxy matrix are used. The results are compared with overall responses of tows modeled using homogenized tow properties obtained from micromechanics and FEA as well as explicitly modeled tows containing multiple parallel fibers.

The results of our analysis show dependence of the overall elastic properties on both crimp ratio and the normalized wavelength. Separation of fiber/tow scales is achieved at $\lambda/d = 50$.

Higor Galdino da Silva, Mechanical & Aerospace E., New Mexico State U., Las Cruces, NM
Borys Drach, Mechanical & Aerospace E., New Mexico State U., Las Cruces, NM

INTRODUCTION

Manufacturers of composites materials have been using finite element analysis to study the materials' responses under various loading and environmental conditions with the purpose of getting the best performance out of the products when they leave the production line. However, 3D woven composites in particular are difficult to model and analyze due to the complicated shape of the reinforcement fiber tows (bundles of fibers). Moreover, each tow contains thousands of fibers, which makes it almost impossible to represent the tows explicitly in numerical modeling. The standard way of dealing with this difficulty is to apply homogenization theories, e.g. Hashin, Chamis, Hashin-Shtrikman bounds, etc., in order to obtain effective mechanical properties of tows and model them as solid homogeneous objects [1]–[5]. As a result, the material is represented by two solid phases – matrix and homogenized tows – and the entire composite can then be analyzed to determine the overall properties. Such a two-step approach has been demonstrated to work for laminates with unidirectional layers [6], [7] and two-dimensional (2D) woven composites [8], [9] , however, a detailed study focusing on the applicability of the approach to highly crimped three-dimensional (3D) woven composites has not been performed to the best of the authors' knowledge.

Figure 1 presents X-ray computed microtomography images obtained from a unit cell of a 3D woven composite with the "1x1 orthogonal" reinforcement architecture, as well as tows and matrix modeled as solid phases based on the imaging. We processed the microtomography data to determine crimp ratio of three types of tows – warp, weft and binder as follows. From the tomography images, we measured amplitude a and wavelength λ of each the tow and calculated the crimp ratio values as $CR = a/\lambda$.

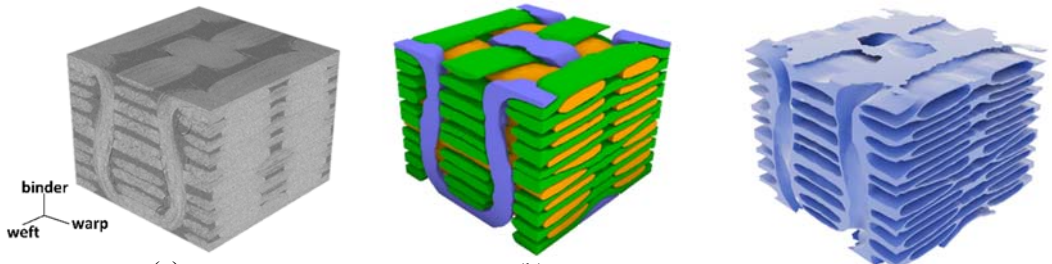

(a) (b) (c)

Figure 1. (a) Microtomography of unit cell; (b) 3D modeled tows; (c) 3D modeled matrix.

Based on our observations, warp tows had negligible waviness and can be safely considered straight (see Figure 2a). On the other hand, weft and binder tows exhibit considerable waviness. For example, crimp ratios of the weft tow shown in Figure 2b and the binder tow shown in Figure 2c were calculated to be 0.12 and 0.39,

correspondingly. The crimp ratios for this 3D woven architecture fall in the range of $0.05 - 0.15$ for the weft and $0.37 - 0.39$ for the binder tows. In addition, based on the fiber diameter (5.2 microns) we estimated the normalized wavelength (λ/d) to be approximately 385 for the highlighted weft tow in the microtomography image shown in Figure 2b.

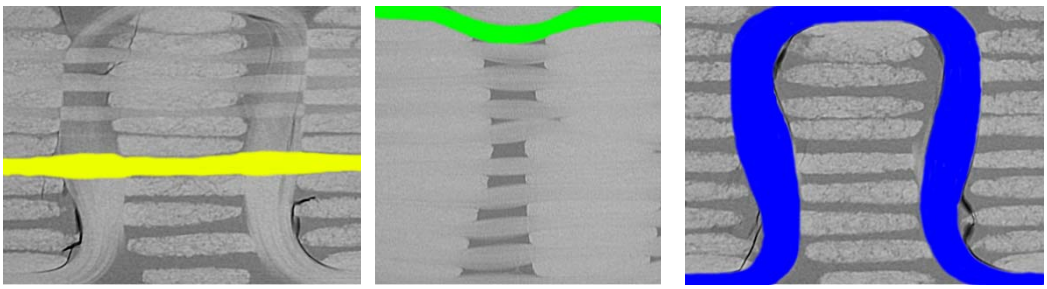

(a) (b) (c)

Figure 2. Highlighted tow paths in a microtomography scan:
(a) warp tow; (b) weft tow; (c) binder tow.

In this paper, we compare Finite Element Analysis (FEA) predictions for effective elastic responses of the explicitly modeled curvilinear tows (curvilinear fibers arranged in a hexagonal pattern and embedded in the matrix material, see Figure 3a) with responses obtained from the homogenized tows (Figure 3b). Three homogenization approaches are considered: micromechanical homogenization based on [10], [11] and FEA homogenization of unidirectional fiber reinforced composites with square and hexagonal fiber arrangements. In our analyses we model the smallest repeating unit of the composite tow called a "unit cell" with the so-called periodic boundary conditions. This allows predicting the overall behavior of the entire tow using a microscale unit containing only one fiber (square arrangement) or five fibers (hexagonal arrangement) instead of all fibers present in the actual tows.

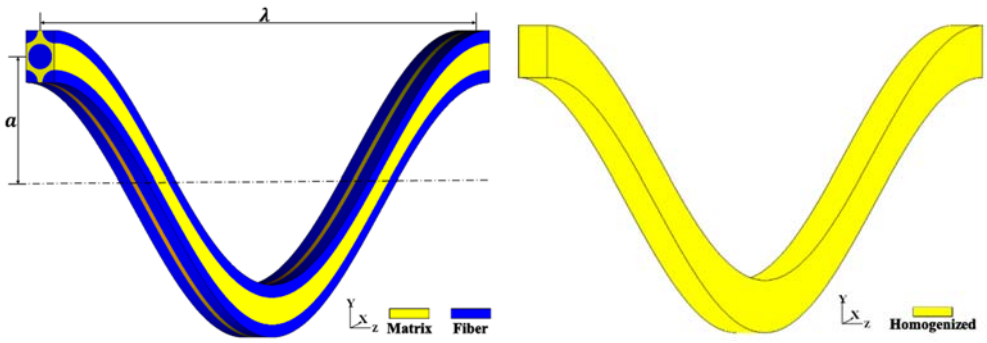

(a) (b)

Figure 3. (a) Amplitude a and wavelength λ shown on an explicit model; (b) homogenized model.

The unit cells used in this paper follow individual fiber paths assumed to have sinusoidal shapes (Figure 3a). Two geometric parameters of the unit cells are considered: crimp ratio (CR) and normalized wavelength (λ/d). The former has been described earlier, the latter is the wavelength λ divided by the fiber`s diameter d. In all of the models discussed, the fiber volume fraction is set to 70%.

FEA MODEL PREPARATION

Geometry and mesh generation

The cross-sections of the FEA models were generated for a given crimp ratio CR and fiber area fraction (AF) specified at the maximum of the tow path, see cross-section I in Figure 4. The considered CR values (0.05, 0.10 and 0.15) represent good estimates for the real values of the tows in 3D woven composites, see Introduction. Note that binder tows are not considered in this analysis due to their non-sinusoidal shape. Since a model's final volume depends on the CR, it is necessary to determine the corresponding AF for each CR value so that the final volume fraction is $VF = 70\%$. In addition to CR, we also varied the normalized wavelength parameter λ/d of the unit cells. The final values of all considered geometric parameters are summarized in Table 1.

Table 1. Geometric parameters of FEA models.

CR	λ/d	d	AF	VF
0.05	5, 10, 20, 50, 100, 150	0.8690	68.49%	70%
0.10	5, 10, 20, 50, 100, 150	0.8416	64.24%	70%
0.15	5, 10, 20, 50, 100, 150	0.8054	58.83%	70%

The geometry and mesh generation procedure that follows is based on [12]–[14]. Using a custom MATLAB script, the cross sections generated in MSC Marc Mentat with Quad4 elements are duplicated along a sinusoidal curve of a given CR. Fiber cross-sections at minima and maxima of the centerline path have circular shapes, while all others are represented by ellipses, see Figure 4. To achieve this, fiber cross-sections at these locations must be deformed during geometry generation, which distorts the surrounding matrix mesh (see II in Figure 4). To eliminate mesh overlapping, Taubin's relaxation [15] is applied to the matrix elements. The final mesh is free of geometric incompatibilities (e.g. element overlap) and structural imperfections (e.g. voids, cracks, etc).

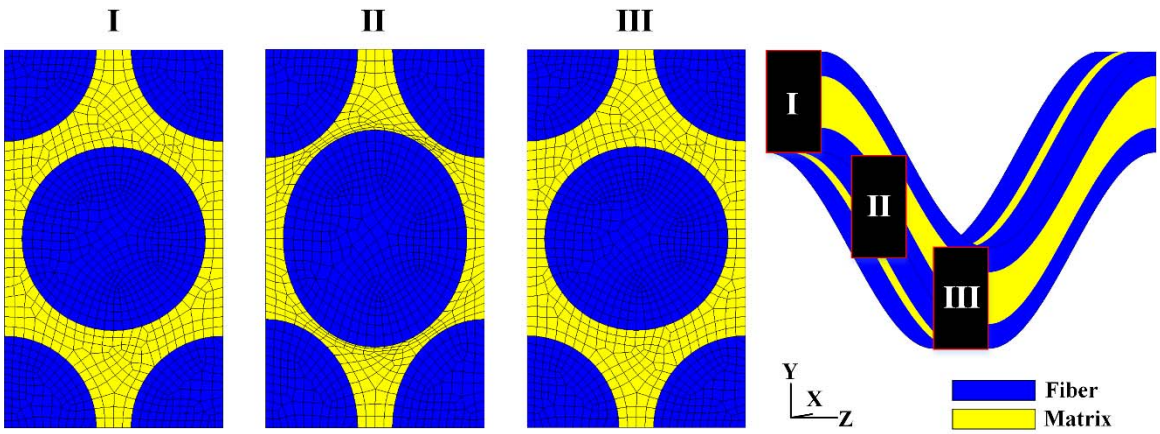

Figure 4. Cross sections of the 3D model with CR=0.15.

The ratio of dimensions of the cross-sections used to generate the models with $CR = 0.05$ and $CR = 0.10$ is equal to the standard value for hexagonal arrangement – $\sqrt{3}$ (Figure 5a, b). Using these cross-sections we were able to achieve 70% final fiber volume fraction without fiber/matrix overlapping. However, it was impossible to generate unit cells with $CR = 0.15$ using the same dimension ratios without overlapping. Therefore we modified the cross-section for $CR = 0.15$ models to the ratio 2.19 (Figure 5c).

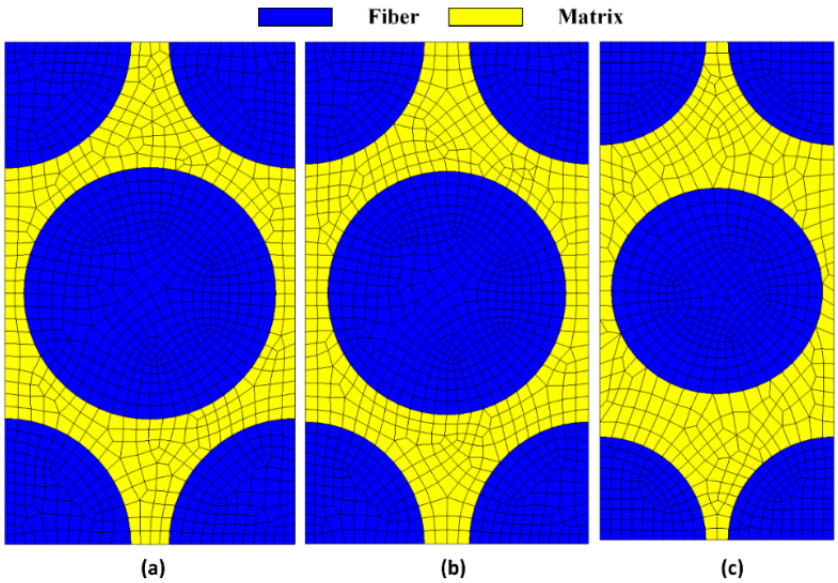

Figure 5. Cross sections used to generate 3D models: (a) $CR = 0.05$; (b) $CR = 0.10$;(c) $CR = 0.15$.

Material properties

Transversely isotropic properties of carbon fibers follow the longitudinal directions. Therefore, to properly apply material properties to a curvilinear fiber, local material orientations must be aligned with the fiber path. In our procedure, orientations are generated in the same MATLAB script mentioned above. Figure 6 illustrates the local material direction 1 (longitudinal fiber direction) in a sinusoidal unit cell meshed with coarse elements; transverse directions 2 and 3 are in the normal plane to longitudinal direction.

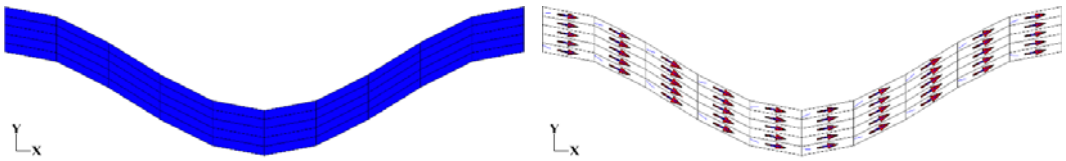

Figure 6. Local material orientations in a 3D unit cell (coarse mesh).

The explicit models (Figure 3a) combine isotropic matrix made of RTM6 resin and transversely isotropic IM7 carbon fibers. Meanwhile, the homogenized models (Figure 3b) are made of the same material whose properties are obtained from formulas presented in [10], [11] or FEA of two unidirectional unit cells – square and hexagonal, see Figure 7. Table 2 presents the elastic properties of the constituents as well as the homogenized properties obtained from all three approaches.

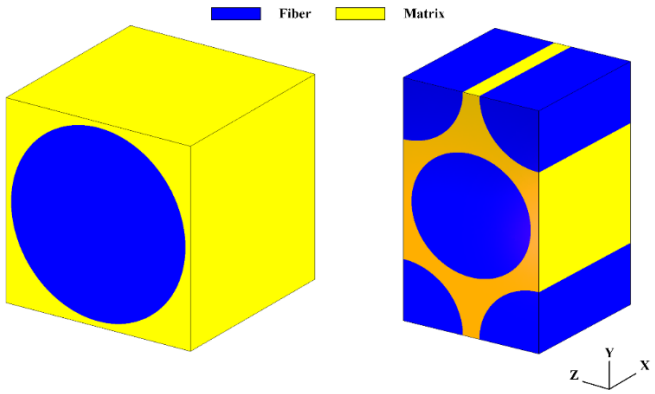

Figure 7. Square unidirectional unit cell (left) and hexagonal unidirectional unit cell (right).

Table 2. Elastic properties of the constituents and homogenized properties of unidirectional tows.

	Constituents		Homogenized		
Material	**Carbon IM7**	**Epoxy RTM6**	**Hashin (1979)**	**Square**	**Hexagonal**
E_1 **(GPa)**	276	2.890	194.067	194.043	194.003
E_2**(GPa)**	23.1	-	10.7087	11.8766	10.2266
E_3 **(GPa)**	23.1	-	10.7087	11.8767	10.2261
ν_{12}	0.35	0.3500	0.3500	0.3501	0.3501
ν_{23}	0.30	-	0.3638	0.3218	0.3942
ν_{31}	0.0293	-	0.0193	0.0214	0.0184
G_{12} **(GPa)**	27.60	1.070	5.0070	5.9762	5.0953
G_{23} **(GPa)**	8.885	-	3.9260	3.1649	3.6705
G_{31} **(GPa)**	27.60	-	5.0070	5.9761	5.0948

Boundary conditions

To preserve periodicity of the analyzed unit cells during deformation, periodic boundary conditions (PBCs) are applied to all surfaces of the explicit and homogenized models. The PBCs relate displacements of two nodes on opposite faces of a unit cell as follows:

$$\mathbf{u}_{x_i+} - \mathbf{u}_{x_i-} = \boldsymbol{\delta}_{x_i} \quad (i = 1, 2, 3) \tag{1}$$

where $\mathbf{u}_{x_i^+}$ and $\mathbf{u}_{x_i^-}$ are displacement vectors of two nodes on the positive and negative x_i faces of a unit cell, respectively, and $\boldsymbol{\delta}_{x_i}$ is the average displacement applied between the faces. Use of periodicity enables modeling the behavior of a large-scale tow using a single unit cell [12]–[14], see Figure 8. Periodic boundary conditions are implement in MSC Marc & Mentat using “servo-links”.

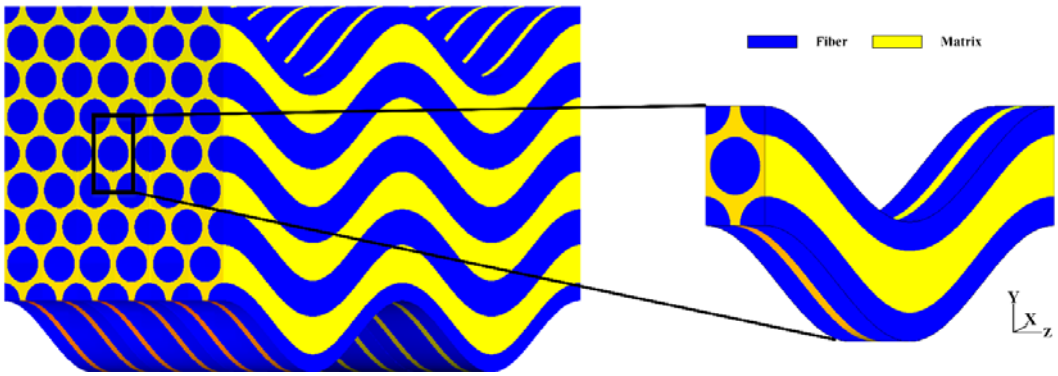

Figure 8. Unit cell compared to a large piece of material.

To obtain the effective elastic properties of the tows, six load cases are applied: three tensile and three shear cases. Figure 9 shows the distribution of the stress component σ_{11} (MPa) in a unit cell with $CR = 0.10$, $\lambda/d = 20$ and material properties given in Table 2 for the applied strain $\varepsilon_{11} = 0.001$.

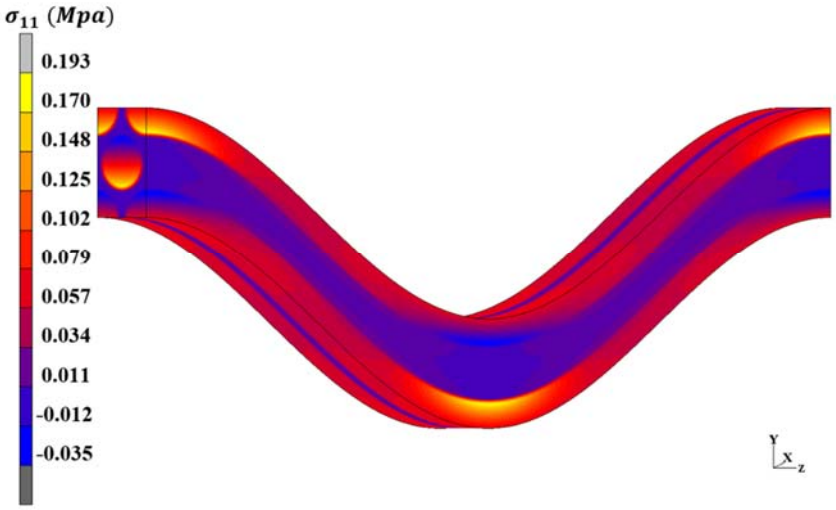

Figure 9. Distribution of the stress component σ_{11} in an explicit model with $CR = 0.10$ and $\lambda/d = 20$.

Processing of the results

The result files from each load case are used to calculate the effective elastic properties via a custom Python script, which considers the components of the stress tensor of each element and its volume to obtain the volume-averaged stress:

$$\langle \sigma_{ij} \rangle_k = \frac{1}{V} \sum_z \left(\sigma_{ij}^{(z)} \right)_k v^{(z)}, \qquad (i,j = 1,2,3; k = 1, \dots, 6) \qquad (2)$$

where $\langle \sigma_{ij} \rangle_k$ is the volume average of the stress component ij calculated from the kth load case, V is the total volume of the model, $\left(\sigma_{ij}^{(z)}\right)_k$ is the stress component ij of the element z calculated from the kth load case, and $v^{(z)}$ is the volume of the finite element number z [16], [17].

RESULTS AND DISCUSSION

The effective Young's modulus E_1, E_2, and shear modulus G_{12} are presented in this section for the set of explicit and homogenized models with geometric parameters presented in Table 1.

Figure 10 presents a comparison of the effective Young's modulus E_1 obtained from FEA simulations of explicit models with the results of the homogenized models for $CR = 0.05$, 0.10 and 0.15. From the figures we conclude that the overall E_1 decreases to an asymptotic value with increase in the normalized wavelength λ/d. It is also clear that E_1 decreases with increase in CR. For all three considered CR values, the results from the homogenized models based on the analytical formulas [10], [11] and FEA homogenization with hexagonal fiber arrangement are virtually the same – 0.9%, 0.8% and 0.3% relative difference for CR values of 0.05, 0.10 and 0.15, respectively. The results obtained from the homogenized model based on the square arrangement, when compared to the hexagonal models, are consistently higher with the difference of 10.5%, 14.2% and 15.1% for CR values of 0.05, 0.10 and 0.15, respectively.

It can be seen that the explicit model predictions converge to the homogenized analytical (hexagonal) values at $CR = 0.05$. Meanwhile, at $CR = 0.10$ and $CR = 0.15$ the explicit model predictions converge to the homogenized square model values. At $CR = 0.05$, the difference between the explicit values and homogenized square values at $\lambda/d = 150$ is -6.7%, and the difference between the explicit model values and the hexagonal model's values is 3.4%. For the crimp ratio of 0.10, the difference between explicit and square, and the difference between explicit and hexagonal are 0.5% and 12.9%, respectively. At crimp ratio of 0.15, the difference between explicit and square, and the difference between explicit and hexagonal are -2.6% and 10.9%, respectively.

Another behavior that can be seen in Figure 10 is that the explicit model predictions converge to the asymptotic value at $\lambda/d = 50$. The difference between the values at $\lambda/d = 50$ and $\lambda/d = 150$ is 1.1%, 1.5%, and 2.6% for crimp ratios 0.05, 0.10, and 0.15, respectively. Therefore, it can be said that the "infinitely" long fiber predictions are attained at $\lambda/d = 50$ for the crimp ratios discussed. The two-step homogenization method requires separation of fiber and tow length scales. In this case, the tow's length scale is several orders of magnitude greater than fiber's length scale.

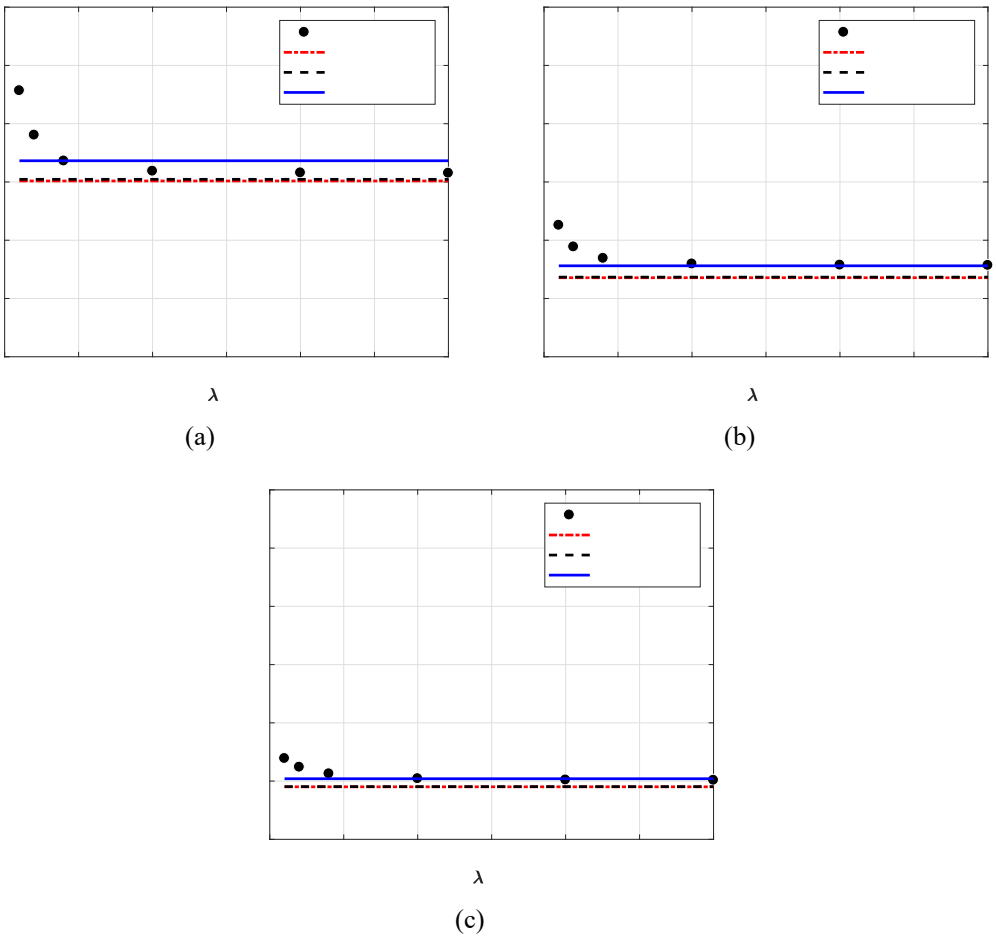

Figure 10. Young's modulus E_1: (a) CR = 0.05; (b) CR = 0.10; (c) CR = 0.15.

Similarly to the Young's modulus E_1, the transverse Young's modulus E_2 also decreases to an asymptotic value as λ/d increases, however, in contrast to E_1, E_2 increases as crimp ratio CR increases, see Figure 11. The sensitivity of E_2 to λ/d appears to increase with CR. The explicit model predictions converge to the homogenized hexagonal, analytical and square predictions at crimp ratios $0.05, 0.10$ and 0.15 with relative errors of 0.7%, 2.3% and -4.5%, correspondingly.

Homogenized analytical, square and hexagonal models result in three different predictions for E_2. However, it is clear that as crimp ratio CR increases, the difference between the homogenized hexagonal and homogenized analytical decreases, the differences are 4.1%, 3.0%, and 1.9% for crimp ratios $0.05, 0.10,$ and 0.15, respectively. Similar to E_1, homogenized square model resulted in the highest predictions among the homogenized models.

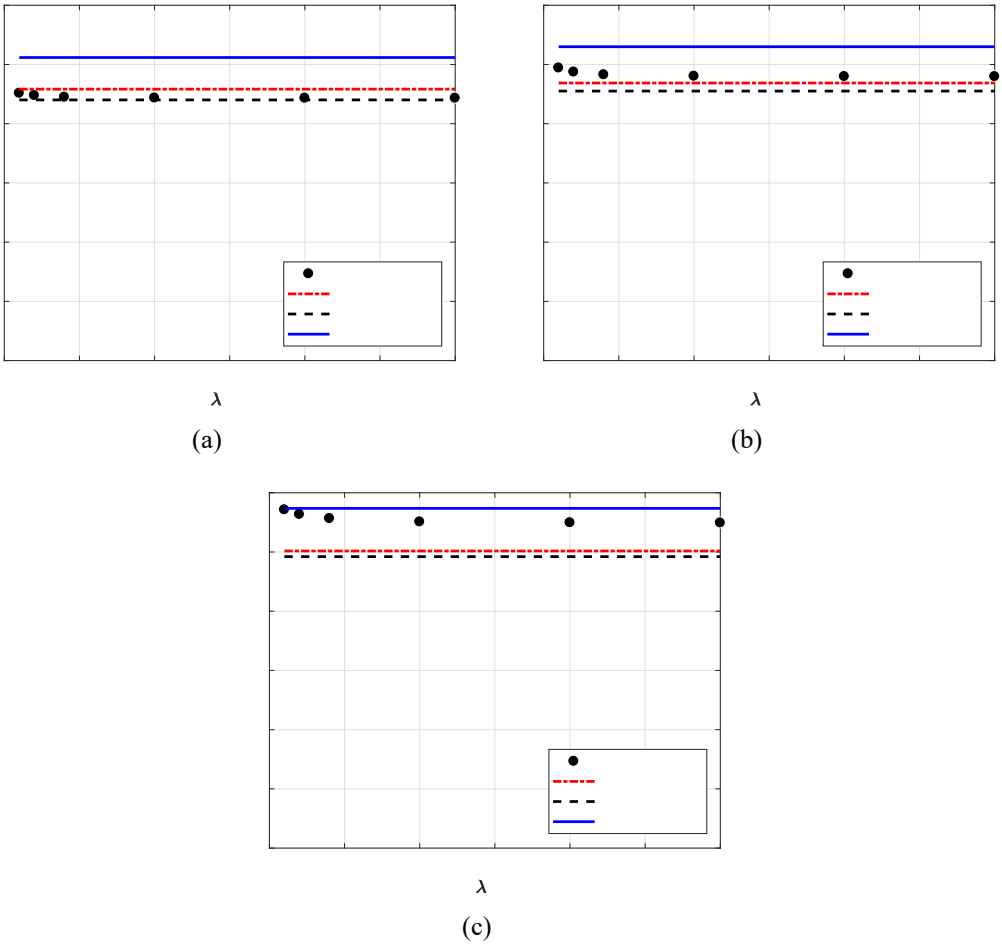

Figure 11. Young's modulus E_2: (a) CR = 0.05; (b) CR = 0.10; (c) CR = 0.15.

As with the Young's modulus E_2, the shear modulus G_{12} increases as CR increases, see Figure 12. At the lowest considered crimp ratio 0.05, G_{12} does not appear to exhibit any sensitivity to the λ/d ratio (Figure 12a). However, the sensitivity increases considerably at $CR = 0.10$ and 0.15 (Figure 12b, c). Similarly to the results for E_1, homogenized analytical and homogenized hexagonal models' predictions are indistinguishable (maximum relative difference is 1.4%). Again, the homogenized square model's predictions are considerably higher than the other two homogenized predictions.

The explicit model's predictions converge to the homogenized analytical (hexagonal) model at $CR = 0.05$ and 0.10. However, at CR = 0.15 the explicit model results in predictions significantly lower than any considered homogenized models' predictions.

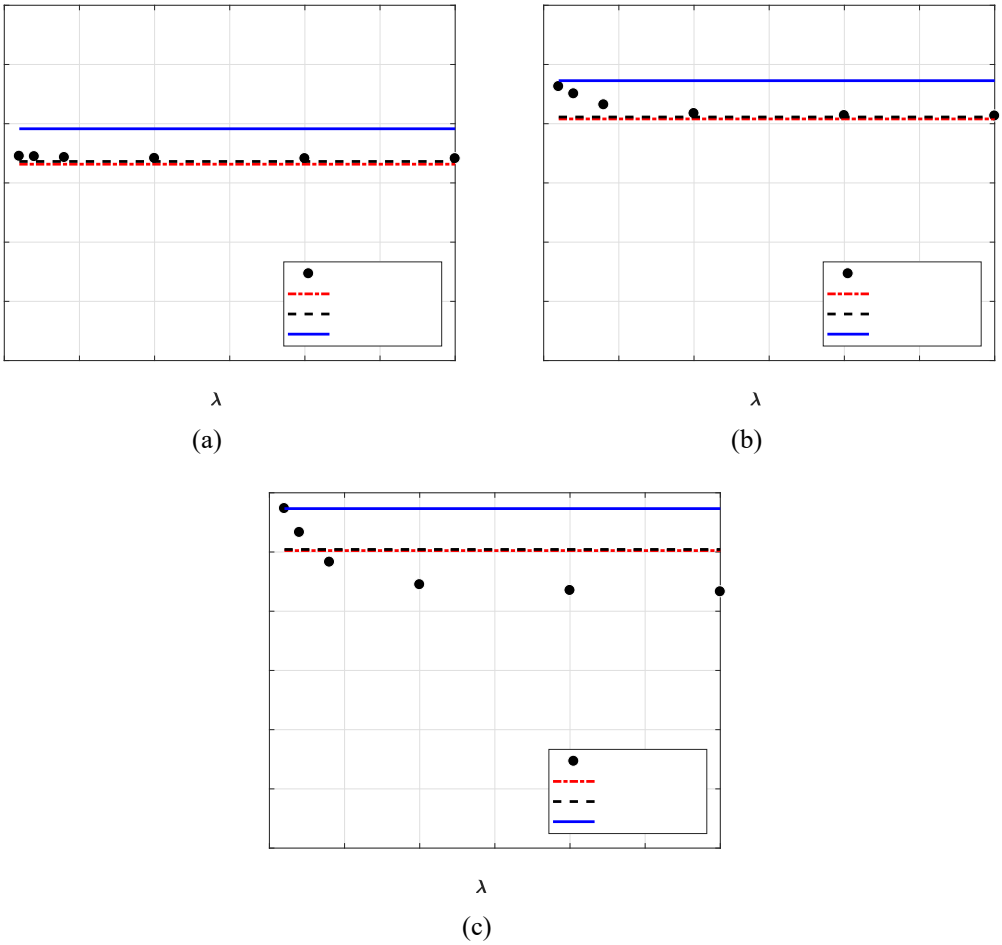

Figure 12. Shear modulus G_{12}: (a) CR = 0.05; (b) CR = 0.10; (c) CR = 0.15.

The remaining elastic properties including the transverse Young's modulus E_3, shear modulus G_{23}, and shear modulus G_{31} did not exhibit dependence on the normalized wavelength λ/d and very little dependence on the crimp ratio (see Table 3), therefore plots of these engineering constants are not presented here. According to Table 3, the homogenized hexagonal model gives the best estimate for E_3 predictions compared with the explicit model – the maximum relative error is 6.4%. On the other hand, homogenized analytical predictions are closest to the explicit model results for G_{23} and G_{31} – the maximum relative errors are 5.0% and 7.1% for G_{23} and G_{31}, correspondingly.

Table 3. Effective elastic properties (GPa).

	Crimp Ratio	Explicit	Homogenized Analytical	Homogenized Hexagonal	Homogenized Square
E_3	0.05	10.10	10.71	10.23	11.88
	0.1	9.83	10.72	10.24	11.89
	0.15	10.97	10.75	10.27	11.91
G_{23}	0.05	3.78	3.97	3.72	3.24
	0.1	4.05	4.06	3.84	3.42
	0.15	4.15	4.18	3.98	3.66
G_{31}	0.05	4.97	4.96	5.03	5.85
	0.1	4.81	4.84	4.87	5.53
	0.15	5.07	4.71	4.70	5.17

CONCLUSIONS

In this paper, we examined the applicability of the two-step elastic homogenization approach to 3D woven composite materials with high crimp ratios. We utilized finite element analysis to compare the effective elastic response of tows having homogenized properties (obtained from analytical and numerical homogenization via FEA) with the response of explicitly modeled tows. To reduce the complexity of the problem we assumed tows to be comprised of repeating unit cells which enabled us to use periodic boundary conditions and represent large tows having thousands of fibers with a single unit cell having only five fibers arranged in a hexagonal pattern.

Our results are presented as plots of effective engineering moduli vs the normalized wavelength parameter λ/d which describes the relative dimension of a single fiber with respect to the tow. The properties were calculated for three values of crimp ratios CR – 0.05, 0.10 and 0.15 (values are based on microtomography analysis of 3D woven carbon/epoxy composite, see Introduction) – and six values of λ/d – 5, 10, 20, 50, 100 and 150.

The asymptotic values of the effective moduli considered in this paper exhibit different characteristics of dependence on crimp ratio. As the crimp ratio increases, E_1 decreases; E_2, G_{12} and G_{23} increase; E_3 and G_{31} do not exhibit significant changes. These trends are in agreement with previously published results [17]–[19].

It was observed that constants E_1, E_2 and G_{12} decrease with increasing λ/d, while E_3, G_{23} and G_{31} do not exhibit any significant dependence on λ/d. At the same time, analysis showed that the constants that do depend on the normalized wavelength reach their asymptotic values in the vicinity of $\lambda/d = 50$ which is well below the normalized wavelengths of carbon/epoxy 3D woven composites as is shown in the

Introduction. This means that the separation of scales required for two-step homogenization can be safely assumed for these composites.

However, it is not immediately clear which homogenization scheme should be used, because there is no one model that predicts the explicit model's behavior for all six elastic moduli. While the homogenized hexagonal and homogenized analytical models are close to each other in all predictions of the considered Young's and shear moduli, they appear to work for predicting explicit model's response (asymptotic value) for E_1 ($CR = 0.05$), E_2 ($CR = 0.05, 0.10$), G_{12} ($CR = 0.05, 0.10$), E_3 (all crimp ratios), G_{23} (all crimp ratios) and G_{31} ($CR = 0.05, 0.10$). For all other combinations (except G_{12} at $CR = 0.15$) the homogenized square model works best.

Finally, the two-step homogenization appears to be applicable to high crimp 3D woven composites with crimp ratios in the range $0 - 0.15$, however, for the best results we recommend obtaining effective elastic moduli as functions of CR via explicit model analysis for $\lambda/d = 50$. The next best alternative is to use analytical homogenization formulas [10], which appear to work well for most elastic moduli/crimp ratio combinations and do not require additional finite element calculations.

ACKNOWLEDGEMENTS

This material is based upon work supported by the National Science Foundation under Grant No. CMMI-1662098.

REFERENCES

[1] I. Verpoest and S. V. Lomov, "Virtual textile composites software WiseTex: Integration with micro-mechanical, permeability and structural analysis," *Compos. Sci. Technol.*, vol. 65, no. 15–16 SPEC. ISS., pp. 2563–2574, 2005.

[2] A. Drach, B. Drach, and I. Tsukrov, "Processing of fiber architecture data for finite element modeling of 3D woven composites," *Spec. Issue Dedic. to Profr. Zdeněk Bittnar Occas. his Seventieth Birthd. Part 2*, vol. 72, pp. 18–27, 2014.

[3] X. Liu, K. Rouf, B. Peng, and W. Yu, "Two-step homogenization of textile composites using mechanics of structure genome," *Compos. Struct.*, vol. 171, pp. 252–262, 2017.

[4] C. Fagiano, M. Genet, E. Baranger, and P. Ladevèze, "Computational geometrical and mechanical modeling of woven ceramic composites at the mesoscale," *Compos. Struct.*, vol. 112, no. 1, pp. 146–156, 2014.

[5] B. Tomkova, M. Sejnoha, J. Novak, and J. Zeman, "Evaluation of Effective Thermal Conductivities of Porous Textile Composites," *Int. J. Multiscale Comput. Eng.*, vol. 6, no. 2, pp. 153–167, 2008.

[6] R. Quelho, D. M. Rafael, T. Luiz, and D. Jose, “Elastic properties of unidirectional fiber-reinforced composites using asymptotic homogenization techniques,” *J. Brazilian Soc. Mech. Sci. Eng.*, vol. 9, 2018.

[7] R. Q. de Macedo, R. T. L. Ferreira, J. M. Guedes, and M. V. Donadon, “Intraply failure criterion for unidirectional fiber reinforced composites by means of asymptotic homogenization,” *Compos. Struct.*, vol. 159, pp. 335–349, 2017.

[8] S. V. Lomov *et al.*, “Predictive analyses and experimental validations of effective elastic properties of 2D and 3D woven composites,” *13th Eur. Conf. Compos. Mater.*, 2008.

[9] D. Olave, Mireia, Vanaerschot, Andy, Lomov, Stepan V., Vandepitte, “Internal Geometry Variability of Two Woven Composites and Related Variability of the Stiffness,” *Polym. Compos.*, vol. 33, no. 8, pp. 1335–1350, 2012.

[10] Z. Hashin, “Analysis of properties of fiber composites with anisotropic constituents,” *J. Appl. Mech.*, vol. 46, no. September 1979, pp. 543–550, 1979.

[11] Z. Hashin, “Analysis of Composite Materials— A Survey,” *J. Appl. Mech.*, vol. 50, no. Ref 4, pp. 481–505, 1983.

[12] J. S. and J. Llorca., “A numerical approximation to the elastic properties of sphere reinforced composites.,” *J. Mech. Phys. Solids*, vol. 50, pp. 21017–2121, 2002.

[13] B. Drach, I. Tsukrov, and A. Trofimov, “Comparison of full field and single pore approaches to homogenization of linearly elastic materials with pores of regular and irregular shapes,” *Int. J. Solids Struct.*, vol. 96, pp. 48–63, 2016.

[14] Z. Xia, Y. Zhang, and F. Ellyin, “A unified periodical boundary conditions for representative volume elements of composites and applications,” *Int. J. Solids Struct.*, vol. 40, no. 8, pp. 1907–1921, 2003.

[15] G. Taubin, “A signal processing approach to fair surface design,” *Proc. 22nd Annu. Conf. Comput. Graph. Interact. Tech. - SIGGRAPH ’95*, pp. 351–358, 1995.

[16] D. Kuksenko and B. Drach, “Effective conductivity of materials with continuous curved fibers,” *Int. J. Eng. Sci.*, vol. 118, pp. 70–81, 2017.

[17] B. Drach, D. Kuksenko, and I. Sevostianov, “Effect of a curved fiber on the overall material stiffness,” *Int. J. Solids Struct.*, vol. 100–101, pp. 211–222, 2016.

[18] M. R. Garnich and G. Karami, “Finite element micromechanics for stiffness and strength of wavy fiber composites,” *J. Compos. Mater.*, vol. 38, no. 4, pp. 273–292, 2004.

[19] J. Zhu, J. Wang, and L. Zu, “Influence of out-of-plane ply waviness on elastic properties of composite laminates under uniaxial loading,” *Compos. Struct.*, vol. 132, pp. 440–450, 2015.